Would a Mighty Smack Tilt Uranus?

Louis Eddershaw
University of Bristol, H.H. Wills Physics Laboratory, Tyndall Avenue, Bristol BS8 1TL, UK

17 April 2024

ABSTRACT

The parameters of a single giant impact event resulting in Uranus' characteristic axial tilt of 97.77° are investigated with a number of Smoothed Particle Hydrodynamics (SPH) simulations using the SWIFT hydrodynamics code. The minimum mass of the impacting body needed to induce the axial tilt, as well as the required impact geometry are presented. Using a pre-rotating young Uranus with a period of 16.87 hours, and an impactor of similar material composition, a minimum impactor mass of 0.7 $M_\oplus$ is required to produce the required axial tilt, although the impact remnant is left spinning significantly slower than Uranus' current rate of rotation. Additionally, considerations of the post-impact dynamics of the remnant suggest a maximum impactor mass of 1.75 $M_\oplus$ before the resulting remnant is left spinning too quickly to agree with current observations of the planet. The impact geometry required for successful collisions suggests the impactor would need to be on a reasonably eccentric orbit around the Sun and may require interactions from the other giant planets to establish its impact trajectory. A discussion of the applicability of rigid-body calculations that are utilised in SPH studies of this type is also presented.

1 INTRODUCTION

Unlike most of the planets in the Solar System, Uranus spins on its side. With an axial tilt of 97.77°, its rotational axis points nearly perpendicular to its orbital axis (Figure 1). For years, the highly unusual circumstance Uranus finds itself in has brought about speculation of the planet's history. One of the leading hypotheses for the curious axial tilt proposes a giant impact in the early stages of its life (Safronov 1972; Slattery et al. 1992; Kegerreis et al. 2018, 2019; Ida et al. 2020; Rufu & Canup 2022). A giant impact typically refers to a collision between objects of planetary proportions, but this definition can sometimes be extended to collisionless, near-miss events in which tidal deformation 'impacts' the bodies. In Uranus' case, a giant collision could deliver a significant amount of angular momentum along a new axis and act to change the rotational axis, and therefore axial tilt, of the planet to its current position.

To understand why the rotational and orbital axes of bodies in a planetary system are expected to be similar, the mechanism by which the bodies form should be noted (Giuli 1968; Harris 1977; Harris & Ward 1982). Planetary formation begins when density fluctuations in the disk cause objects to coalesce out of the surrounding material. Both gravitational attraction and collisional accretion of other bodies in the disk then drive some of those objects to grow and become planetesimals. At appreciable sizes, a given planetesimal will tend to see neighbouring planetesimals orbiting more slowly if they are interior of its orbit, and more quickly if they are exterior of it. This difference in velocity from one side of the body to the other induces a rotation when colliding with its neighbours (Figure 2). Impacts on both the interior and exterior sides of its orbit combine to exert a torque about the orbital axis, leaving the planetesimal with a rotation in the same sense as that of the planetary disk. Asymmetries in the collisions on either side of the planetesimal can cause slight tilts of the rotational axis from the orbital axis but deviation as extreme as Uranus' is empirically rare[1].

[1] NASA Goddard Space Flight Center: http://nssdc.gsfc.nasa.gov/planetary/factsheet/

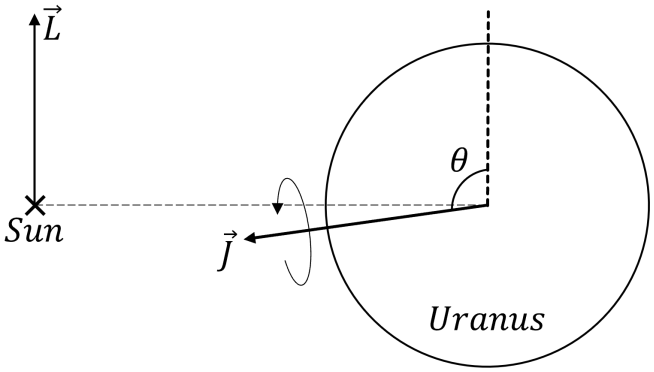

Figure 1. The rotational angular momentum axis $\vec{J}$ of Uranus is distinctly misaligned with its orbital angular momentum axis $\vec{L}$. Its axial tilt θ is approximately 97.77°. Uranus orbits the Sun in the plane going into and out of the page.

The collisional mechanism by which planets are thought to be spun into their rotation appears to lend itself naturally to the impact hypothesis, which is likely the reason this hypothesis is favoured by many. However, it does not stand unopposed; a collisionless theory states that complex resonances between the rotations and orbits of several objects in the Solar System can also push Uranus on its side (Harris & Ward 1982; Boué & Laskar 2010; Rogoszinski & Hamilton 2021). The torques induced on a body due to tidal deformation from the Sun can cause a planet's rotational axis to precess about its orbital axis. The rate of this precession can couple with the precession of the orbital axis itself, due to torques from other bodies in the Solar System, to produce a resonance; a regular gravitational influence that can amplify the precession of the rotational axis and induce reasonably large axial tilts. This complex dynamical behaviour has been used to explain Saturn's (much smaller) axial tilt (Hamilton & Ward 2004), which might suggest 'spin-orbit resonances' are applicable to Uranus. However, as well as some resonance models still requiring collisions to explain Uranus' tilt (Rogoszinski & Hamilton

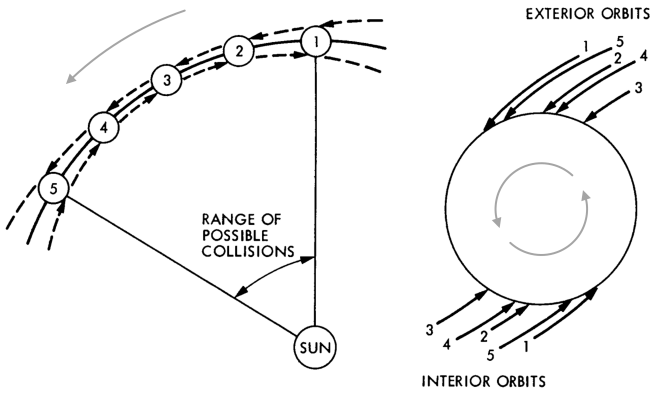

Figure 2. A schematic of how collisional accretion onto a protoplanet induces a rotation in the same sense as the protoplanet's orbit. The protoplanet ascends through the numbered locations on the left, anti-clockwise around the Sun. The impacts at each orbital location are denoted on the planet-centred diagram on the right. This diagram is republished, and lightly adapted, from Harris (1977).

2021), the implications of the existence and behaviour of Uranus' satellite system presents an issue for resonance models; an axial tilt of over 90° might suggest the satellites should be orbiting Uranus in the opposite sense to the planet's rotation, which they are not seen to do (Lubow et al. 1999). Impact hypotheses are also more successful at suggesting explanations of additional qualities exhibited by the ice giant; the apparent lack of heat flow from its centre (Nettelmann et al. 2016; Podolak et al. 2019), the tilt of its magnetic axis which is neither aligned with its rotational nor orbital axis (Ness et al. 1986) and an explanation that its satellite system may have been significantly affected by a giant impact launching material into orbit (Ida et al. 2020; Rufu & Canup 2022).

Safronov (1966, 1972) was the first to suggest that the ice giant was formed from impacts with large bodies (impactors) that were scattered onto colliding paths by Jupiter, which could have had masses as large as 0.07 times the mass of Uranus, or roughly 1 $M_\oplus$ ($M_\oplus = 1$ Earth mass).

With Slattery et al. (1992), increasing computational power allowed for some of the first particle simulations of giant impacts with the young protoplanet. These simulations had a resolution of 8000 particles (5000 to represent the planet, and 3000 to represent its impactor), or 2×10^{-3} $M_\oplus$ per particle. Uranus was modelled as non-rotating before impact, and collisions that left the planet spinning with a rotational period that was, at most, today's value (17.24 hours; Warwick et al. 1986) were sought. These criteria were imposed under the assumption that the post-impact Uranus would interact magnetically with external material that would act to slow the planet's rotation towards its current state. With these assumptions, it was concluded that a bare minimum impactor mass of 1 $M_\oplus$ was required.

Kegerreis et al. (2018) conducted a series of similar simulations with significantly improved resolutions of 10^5 and 10^6 particles, or 10^{-4} and 10^{-5} $M_\oplus$ per particle. With the increase in resolution, it was concluded that at least a 2 $M_\oplus$ impactor is needed to leave Uranus spinning faster than it is today. In a similar fashion to the previous literature, there was no pre-impact rotation of the protoplanetary Uranus.

In Rufu & Canup (2022), the considerations of pre-impact rotation in the protoplanet were discussed, alongside an accretion model of the formation of the satellites. The formation of Uranus' satellite system appeared to be inconsistent with certain impact scenarios, but the detailed mechanism by which the system evolves and forms is still partially unknown, and there remains scope to investigate further impacts.

In the study presented here, new simulations of giant impacts with a rotating protoplanet are used to investigate and constrain the parameters needed to obtain Uranus' characteristic axial tilt. This study aims to combine the approaches of the previous literature (Kegerreis et al. 2018 and Rufu & Canup 2022) by considering pre-impact rotation and its effect on the minimum impactor mass required to reproduce Uranus' axial tilt.

2 METHODS

2.1 Smoothed Particle Hydrodynamics and SWIFT

In events like giant impacts, the gravitational strength of large, planet-sized objects far outweigh the material strength of the bodies themselves, and thus objects of this size are reasonably approximated as fluids (Benz 1988). Fluid dynamics, or hydrodynamics, can be simulated with various computational methods, and the research in this study was completed with Smoothed Particle Hydrodynamics (SPH); a Lagrangian approach to CFD (Gingold & Monaghan 1977; Lucy 1977). The SWIFT astrophysical code[2] uses SPH methods to conduct planetary simulations (Schaller et al. 2024), and was used in similar studies of Uranus in Kegerreis et al. (2019).

As opposed to Eulerian approaches to CFD, which divide the environment space into a dynamic mesh and compute the flow of material between mesh cells (Trac & Pen 2003), Lagrangian approaches discretise the material into particles and evolve them through a fixed space (Benz 1988). Developed by Gingold & Monaghan (1977) and Lucy (1977), the core of SPH simulations is the smoothing process. Since spatial information for a given quantity $A(\boldsymbol{r})$, say pressure, is only initially well-defined at the particles' positions, in order to recover a continuous distribution of pressure, its value must be interpolated for regions between particles. A particle can be thought of as a kind of Dirac delta function for each of the quantities it carries, but the kernel $W(\boldsymbol{r}, h)$ acts to smooth the particle quantities out over space according to h, the characteristic smoothing length. The bridge between discrete and continuous representation of the quantity $A(\boldsymbol{r})$ is supported by the so-called 'integral interpolant' $A_I(\boldsymbol{r})$, expressed as

$$A_I(\boldsymbol{r}) = \int_{\text{all space}} A(\boldsymbol{r'}) W(\boldsymbol{r} - \boldsymbol{r'}, h) \mathrm{d}\boldsymbol{r'}, \tag{1}$$

where the kernel acts to estimate $A_I(\boldsymbol{r})$ by weighting the contribution of A from nearby points. The kernel satisfies the following two conditions,

$$\int_{\text{all space}} W(\boldsymbol{r} - \boldsymbol{r'}, h) \mathrm{d}\boldsymbol{r'} = 1, \tag{2}$$

$$\lim_{h \to 0} W(\boldsymbol{r}, h) = \delta(\boldsymbol{r}), \tag{3}$$

where $\delta(\boldsymbol{r})$ is the Dirac delta function in 3 dimensions. The form of the kernel is often a near-Gaussian spline (Monaghan & Lattanzio 1985), as depicted in Figure 3.

When taking this process to a discrete form, as is the case with numerical simulations and particle representations, the integral interpolant becomes the summation interpolant $A_S(\boldsymbol{r})$. The summation

[2] https://github.com/SWIFTSIM/SWIFT

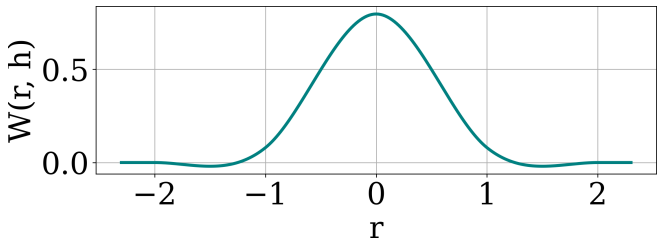

Figure 3. A typical form of the SPH kernel, in 1-dimension, with a characteristic smoothing length h of 1 (unitless). An interactive version of this plot is available here.

interpolant of a given quantity at precisely the location of a given particle, $\boldsymbol{r}_i$ where i denotes the given particle, is then used to define that particle's quantity A_i, i.e.

$$A_s(\boldsymbol{r}_i) = A_i = \sum_k m_k \frac{A_k}{\rho_k} W(\boldsymbol{r}_i - \boldsymbol{r}_k, h_i), \tag{4}$$

where the summation is over all particles k which carry mass m_k, density ρ_k, position $\boldsymbol{r}_k$, and the quantity in question A_k. The factor of m_k/ρ_k represents a volume originating from the infinitesimal volume element $\mathrm{d}\boldsymbol{r'}$ in the previous integrals. Particles can also carry their own smoothing length h_i which allows different particles to be influenced over a different range of distances, depending on the local environment they might find themselves in.

When the particle densities are being calculated, i.e. when A becomes ρ, Equation 4 reduces to

$$\rho_i = \sum_k m_k W(\boldsymbol{r}_i - \boldsymbol{r}_k, h_i). \tag{5}$$

The density of a particle is an important quantity in the SWIFT simulation code; it dictates whether particles should be considered for hydrodynamical interactions or not (Schaller et al. 2024). Since such interactions are computationally costly to evaluate, it is desirable to not waste resources computing, say, pressures exerted between particles that are well separated. In cases where the density carried by a particle drops below this threshold, or 'density floor', it is no longer necessary to compute hydrodynamics *and* ballistics, so the particle simply becomes ballistic; its only contributions to the simulation are its gravitational, or N-body, effects. When the particle density rises above the density floor again, perhaps because it travelled ballistically into a region with many particles, hydrodynamical interactions are switched back on. It is in this way that the numerical artefacts in SWIFT, and some SPH methods in general, begin to creep into simulations; if the density floor is set too high, or particles sit right on the edge of the density floor, then instabilities and subtly odd particle behaviours can arise as a result. Particles that should be interacting hydrodynamically, if only weakly, are sometimes unsuitably represented in the simulations and act to reduce the simulation's physical significance. These effects can be reduced by increasing the number of particles such that any one 'bad' particle is less important to the entire ensemble of simulation particles, but particle systems are computationally expensive to scale up significantly.

Generally, SPH simulations are only informative for general behaviours of particle systems and are less suited to drawing conclusions from any small-scale, or single-particle, dynamics. With the focus of this study being the large-scale rotation of a planet after an impact event, the use of a large number of particles means SPH methods can still provide a reasonable platform from which to analyse these collisional events.

2.2 Equations of State

Since hydrodynamic interactions are at the heart of SPH simulations, the way in which particles react to temperatures and pressures of neighbouring particles could lead to varying results if different materials are considered. In an analysis of impacts onto another gas giant, Saturn, by Korycansky et al. (1991), the retention of its atmosphere is very sensitive to initial conditions; it is the act of modelling the atmosphere as distinct from, say, the core that enables important conclusions to be drawn from such analysis.

Materials can be represented by their Equation of State (or EoS) which describes the relationship between a number of properties in the material, such as internal energy, temperature, density, and pressure. Both analytical and empirical EoSs exist for a wide range of materials, and each type has its advantages and disadvantages. Empirically derived EoSs benefit from being sourced from the real-world behaviour of these materials under a range of conditions; the subtleties of phase transitions and violent vaporisation can be measured directly, but the experiments are costly and are therefore harder to obtain for a wide range of materials (Ross et al. 1981). Analytically derived EoSs can provide an approximation for a number of materials but suffer from the inaccuracies and simplifications of the models that drive them (Hubbard & Marley 1989). Often, empirical results will inform analytical EoSs and these can therefore provide reasonable material representations. For giant impacts, due to the vast amount of energy delivered to the target by the impactor, the dynamics of vaporisation play an important role in the post-impact state, and so empirically sourced, or at least empirically driven, EoSs are favoured where possible.

Relatively little is known about the internal composition of Uranus, but its estimated composition is thought to consist of a hot, and predominantly rocky, core (with magnetic behaviour to explain its magnetic field) surrounded by a volatile, icy mantle, and encased in a hydrogen and helium atmosphere (Podolak & Cameron 1974).

Each particle in the SPH simulation is given a material identifier that allows SWIFT to evaluate the correct response to hydrodynamical effects. The materials/EoSs used in this project were ANEOS Forsterite (Stewart et al. 2020), AQUA (Haldemann et al. 2020), and HM80 HHe (Hubbard & Macfarlane 1980) for the core, mantle, and atmosphere, respectively, of the pre-impact, or proto-, Uranus.

The impactor is assumed to be of similar composition to the proto-Uranus but is modelled without the hydrogen and helium atmosphere. The rock-ice mass ratio is taken to be approximately the same in both bodies, to be consistent with Kegerreis et al. (2018).

2.3 Generating Planetary Profiles

Each of the objects to be simulated undergoing collisions is assumed to be in hydrostatic equilibrium; i.e. they have settled under their own gravity. To generate planetary bodies that satisfy this condition, the WoMa Python library is used. Details of this code are provided in Ruiz-Bonilla et al. (2021).

In a similar fashion to Kegerreis et al. (2018), the combined proto-Uranus and impactor mass is kept constant. This is imposed under the assumption that a negligible amount of mass escapes the system after impact, and therefore the mass of the proto-Uranus is approximately equal to the difference between the current mass of Uranus and the mass of its impactor. As such, for each impactor mass considered, a new protoplanet is generated.

Again following Kegerreis et al. (2018), to generate a model of Uranus in its current state the following boundary conditions are imposed: a pressure of 1 bar, a temperature of 60 K, and an enclosed

mass of 14.54 $M_\oplus$ are defined at a radial distance of 3.98 $R_\oplus$ from Uranus' centre, where 1 $R_\oplus$ = 1 Earth radius. WoMa converges on a model with a rock-ice boundary and an ice-atmosphere boundary radius of 1.01 and 2.72 $R_\oplus$, respectively, yielding masses of 1.63, 11.48, and 1.47 $M_\oplus$ in the rock, ice, and atmospheric layers. The resulting rock/ice mass ratio of 0.14 is then enforced when generating the impactors so as to not disproportionately deliver more of one material than another to the protoplanet.

In contrast to Kegerreis et al. (2018) where Uranus' core had a fixed temperature independent of radial position, the temperature-density relation of the core material is taken to be adiabatic, and defined by a fixed entropy that results in a continuous temperature profile across the core-mantle boundary. The lack of heat outflow from Uranus' centre suggests, due to its low luminosity, that the atmosphere is also adiabatic (Helled et al. 2011), and so this is also assumed in the model. For reference to future models of Uranus, with these methods the core temperature of the current-day Uranus is modelled to be approximately 9000 K. Current predictions of Uranus' actual core temperature vary widely on the order of 10^3 K (Nettelmann et al. 2016; Podolak et al. 2019), so the validity of this model can be tested with an improved understanding in the future. The radial profiles of the current-day Uranus, as well as three proto-Uranus and impactor pairs, are provided in Figure 4.

With stable profiles for the planetary bodies, WoMa can also generate the planets' particle representations (Ruiz-Bonilla et al. 2021). SPH methods require all particles to be of a similar mass in order to not incite any numerical instabilities, so the resolution of each body is proportional to its mass, i.e. for the simulations performed in this study, the combined resolution of approximately 10^6 particles results in a 0.7 $M_\oplus$ impactor and its associated proto-Uranus having resolutions of approximately 4.8×10^4 and 9.5×10^5 particles, respectively. Cross-sectional views of these example particle configurations are given in Figure 5.

2.4 Relaxation Simulations

While WoMa aims to generate as stable a planetary profile as possible, when the particle configurations are constructed the particles might not be in perfect equilibrium. Simulating the initial state with SWIFT can often demonstrate this; where there are sharp changes in density within the planet, such as near material boundaries, unwanted hydrodynamical forces are calculated and particles are accelerated. The shifting of boundary particles can induce oscillations in the entire planet, with the motion only subsiding after many (simulated) hours once natural damping guides the system to its new equilibrium. Letting the particle systems relax to their natural equilibrium can take many real-world hours to simulate, but velocity damping can be employed to converge on a stable configuration more efficiently. With velocity damping, the particle velocities are halved every time step so as to reduce a particle's response to hydrodynamical forces, which limits the amplitude of any oscillation in the planet. Typically, a simulated time of about 4 hours is more than sufficient to qualitatively remove any oscillations; this compares to required simulation times on the order of tens of hours to multiple days without the velocity damping mechanism.

2.5 Establishing Pre-Impact Rotation

In order for an impact's effects on the rotational axis of Uranus to be investigated, Uranus should have pre-impact rotation in order for a change in the rotational axis to be well defined. In the simulations run in this study, only the proto-Uranus bodies have pre-existing rotation; the impactor's angular momentum contributions are purely orbital relative to Uranus at the start of the simulations.

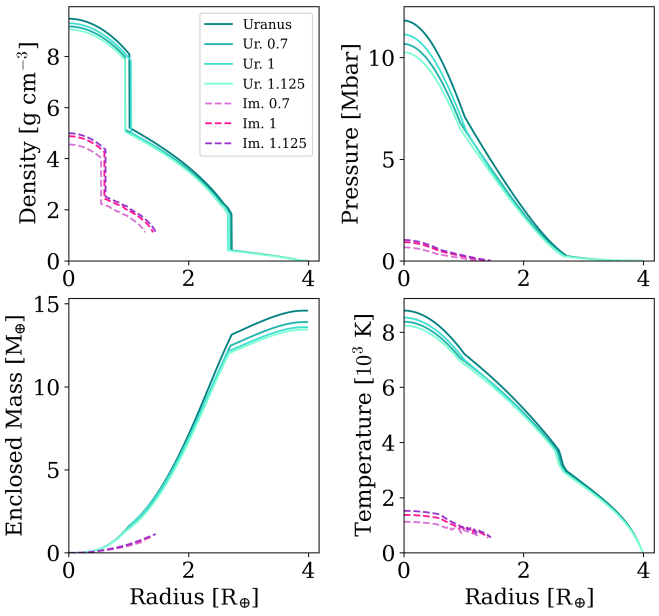

Figure 4. Radial profiles of density, pressure, enclosed mass, and temperature for the Uranus model and 3 proto-Uranus and impactor pairs. The protoplanets are denoted with solid lines, and the impactors are denoted with dashed lines, as in the legend. The numerical values next to the type given in the legend indicate each pair's impactor mass in units of $M_\oplus$.

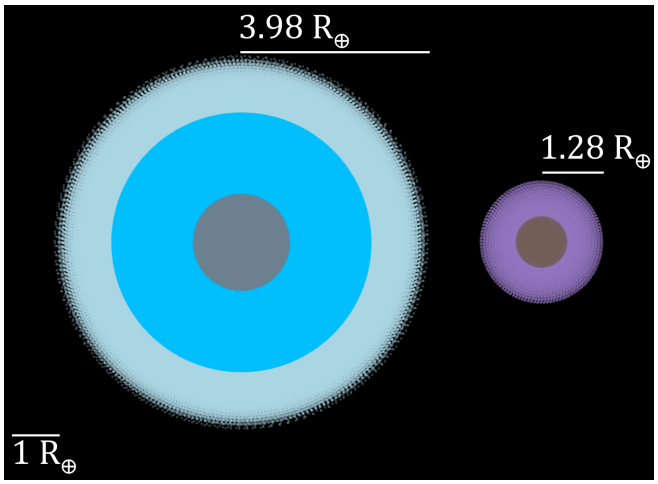

Figure 5. Cross sections of a 13.84 $M_\oplus$ proto-Uranus (left) and a 0.7 $M_\oplus$ impactor (right). The different colours correspond to particles governed by different EoSs and/or particles originating from different bodies, according to a standard colour scheme; grey, blue, and whitish particles correspond to the rock, ice, and atmospheric materials from the proto-Uranus, and the brown and purple particles correspond to the impactor's rock and ice materials. The radius of each body is denoted with the scale bars.

To quantify the rotation of each proto-Uranus, the following equations are used:

$$\vec{L} = \sum_i m_i(\vec{r}_i \times \vec{v}_i), \tag{6}$$

$$I = \sum_i m_i |\vec{r}_i|^2, \tag{7}$$

$$\vec{\omega} = \frac{\vec{L}}{I}, \tag{8}$$

$$P = \frac{2\pi}{|\vec{\omega}|}, \tag{9}$$

where $\vec{L}$ is the total angular momentum of the combined system of particles labelled i with masses m_i, positions $\vec{r}_i$, and velocities $\vec{v}_i$. The moment of inertia I of the system is used to calculate the combined angular velocity $\vec{\omega}$ and subsequent period of rotation P of the particles. It should be noted that the latter two equations only strictly apply to rigidly rotating particle systems, i.e. when there is no relative velocity between any two particles, and therefore these equations are a slight simplification to the non-rigid rotation intrinsic to these simulations. The analysis of the rotation of Uranus both pre- and post-impact is quantified by measuring the angular momentum and angular velocity under this assumption of instantaneous rigid-body rotation.

With the similarities of Uranus and Neptune extending to their icy composition and somewhat similar masses (Guillot 2005), it is assumed that Uranus' pre-impact rotation period was similar to Neptune's at approximately 17 hours. This is, coincidentally, very close to Uranus' current-day rotation rate, and this is potentially supporting evidence for the opposing spin-orbit resonance hypothesis of the planet's tilt.

Rotation is imparted onto each proto-Uranus in one of two ways; with hemispherical offsetting or with rigid-body-like considerations (see Figure 6). In hemispherical offsetting, particles in opposite hemispheres are given velocities in opposite directions yielding a net angular momentum relative to an axis through the planet's centre. The magnitude of the velocity given to each hemisphere is the same and is approximately equal to the speed of the equator of a rigidly rotating solid sphere with a period of 17 hours. When simulating the planet, the hemispheres initially move laterally before hydrodynamic forces cause the particles to be pulled around to eventually settle onto circular paths about a common axis through the planet's centre. Multiple 'spin-ups' are sometimes needed to establish the correct rotation rate in the proto-Uranus. This method, while quick to implement, introduces oscillatory behaviour that propagates around the desired axis of rotation due to the velocity discontinuities across the hemisphere boundaries. These waves and oscillations need to be left to damp themselves out in further simulations. The previous method of relaxation simulation, to damp density discontinuities, cannot be utilised here since damping each particle's velocity would act to halt the required rotation. The damping of these waves must be left to settle naturally in an unaltered simulation. An animation of a proto-Uranus being spun up this way is available in Appendix A.

When rotating particles in a rigid-body-like fashion, each particle is given the correct velocity, both speed and direction, that it would have when rotating as a rigid body. This method attempts to skip over the chaotic initial rotation of the hemispherical method and converge immediately on consistent, steady-state rotation. Relaxation simulations are mostly unnecessary with this method since, except for very minor fluctuations over time, the particles are already co-moving around the same axis. Some centrifugal distortion is expected at the equator, but the ratio of polar and equatorial radii is relatively small

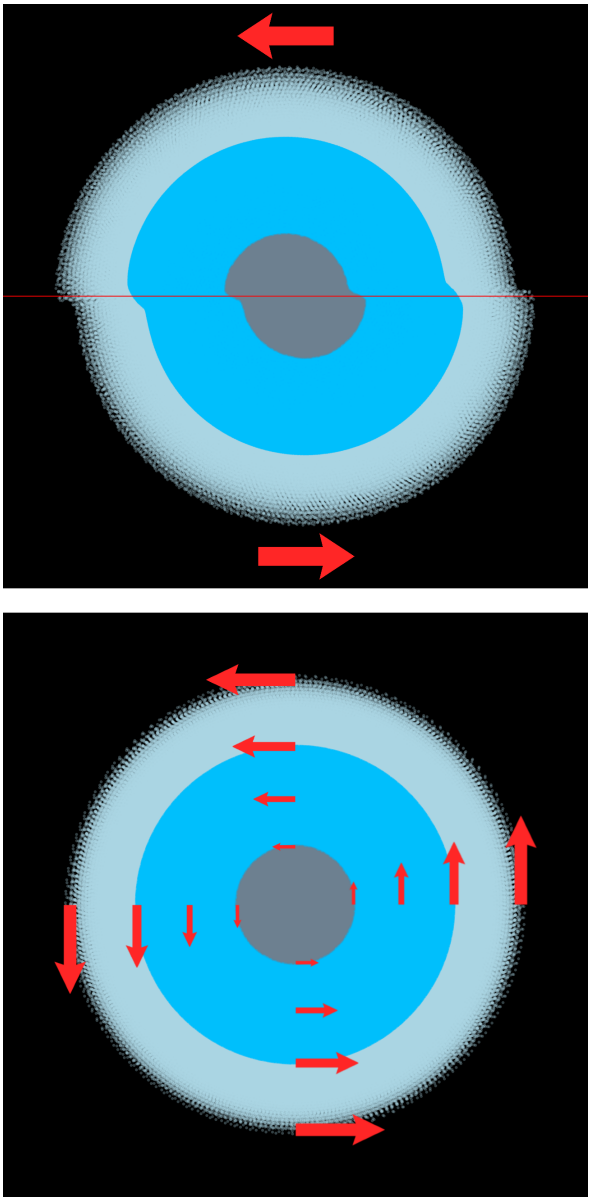

Figure 6. The difference in spin-up methods for the same proto-Uranus. In the top plot, the planet is rotated with the hemispherical offset method, and in the bottom plot the planet is given rigid-body-like rotation. The red arrows indicate the velocity of either an entire hemisphere or example particles, in their relevant plots. Note how the planet is initially deformed with the hemispherical method; a feature that incites oscillation. An animation of a spin up via the hemispherical method is available here.

compared to the other distances in the simulations, and is therefore insignificant against the disruption incurred by a giant impact.

The rigid body method of rotation was only implemented after several impact simulations were set up with the hemispherical method; discrepancies between expected and actual rotation rates of the two methods highlighted the flaws in the assumption that Equations 8 and 9 apply for non-rigid particle systems. The implications of this discrepancy are covered in Sections 3.1 and 4.3.

In Figure 6, the qualitative differences between the two rotation methods are presented. In the hemispherical diagram, the relative motion of each hemisphere is highlighted by depicting the proto-planet approximately 20 minutes from the moment the velocity kick

is applied. The asymmetry between the two hemispheres is what drives hydrodynamic forces to induce rotation in the planet, albeit at the cost of some stability. In contrast, the rigid-body-like method shows no such asymmetry and is far more stable.

2.6 Generating and Simulating Impacts

With a stably rotating proto-Uranus and relaxed impactor, the impacts can now be simulated. To set up the conditions for an impact, WoMa is again used. By providing the impact angle, speed of the impactor at the moment of contact, and the masses and radii of the bodies, the initial configuration of the bodies can be found. WoMa places the target (the proto-Uranus) at the origin and finds the initial velocity required of the impactor such that the velocity at the moment of contact is directed along the negative horizontal axis. The impact angle B is defined as the angle from the horizontal axis that the line connecting the centres of the two bodies makes at the moment of contact (see Figure 7a).

The impactor delivers angular momentum to the proto-Uranus along its relative orbital axis around the planet. In theory, the impactor would also deliver rotational angular momentum along the same axis as the protoplanet's rotation if it were spinning, but impactors in this study have no such rotation. Since WoMa solves the impact conditions for an impact moving towards negative x in the x-y plane, the orbital angular momentum of the impactor is directed along the positive z axis. For the impact to change Uranus' axis of rotation, there must be an initial angular separation ϕ of the impactor's orbital angular momentum and the protoplanet's rotational angular momentum. With a rotational transformation, the protoplanet's particles are adjusted such that these axes are separated. Figure 7b is a side view at the moment of contact, showing the separation of the two axes of angular momentum.

The impactor particles are then offset from the origin by the initial separation of the impactor and target. The initial separation is taken to be 22 $R_\oplus$ such that the gravitational forces on the near side of the impactor to the protoplanet are initially dominated by the impactor's self-gravity when compared to the attraction to the protoplanet at the origin. The impactor particles are then given the calculated velocity of the impactor such that all of the impactor particles will travel together along a trajectory into the target. By moving to the centre of mass frame, the post-impact planet (the impact remnant) should remain near the origin.

The initial condition files are then supplied to SWIFT and the system is evolved accordingly. Computation was performed on BlueCrystal Phase 4, facilitated by the University of Bristol's Advanced Computing Research Centre.

The rotational behaviour and angular momentum of the post-impact system are subsequently determined with Equations 6, 7, 8, and 9.

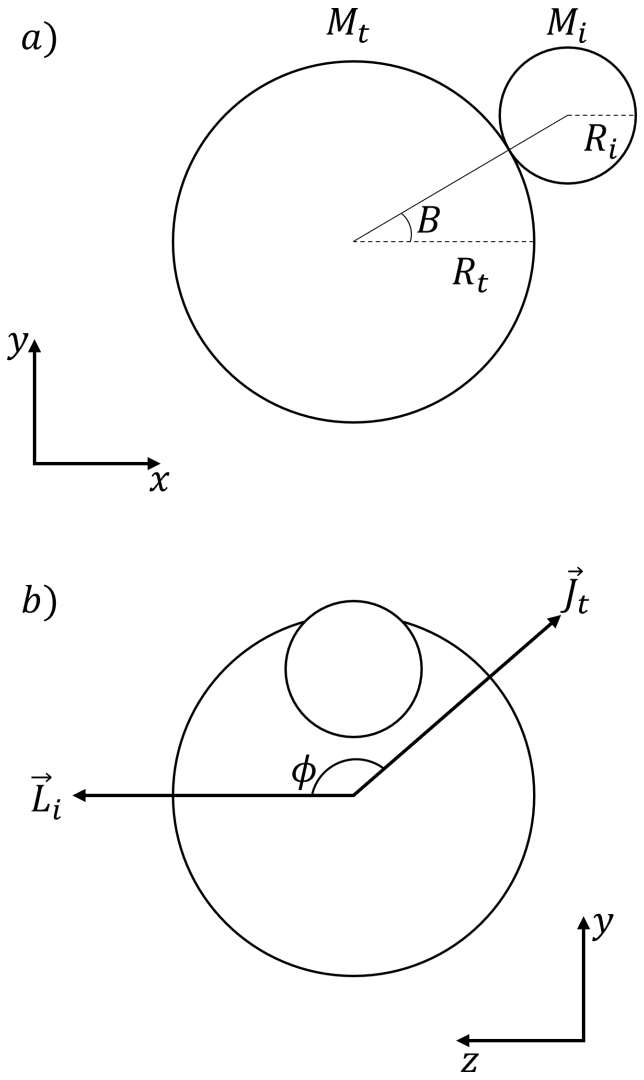

Figure 7. Different perspectives of the impact at the moment of contact. a) Viewing the impact towards negative z, the impactor travels in the negative x direction and makes contact at an angle B from the horizontal axis, where the centre of the target is located at the origin. M and R denote the mass and radius of a body, and subscripts t and i denote target and impactor bodies, respectively. b) Viewing the impact towards negative x, the impactor moves into the page and has an instantaneous orbital angular momentum to the origin of $\vec{L}_i$. The target has rotational angular momentum $\vec{J}_t$ along an axis defined as parallel to its orbital axis. The angular separation of the bodies' angular momentum vectors is denoted ϕ. The magnitudes of the angular momentum vectors are not to scale.

3 RESULTS

The simulations aimed to constrain the parameters that define impacts that sufficiently tilt Uranus' rotational axis by 97.77°. The parameters that were chosen to be 'free' were the mass of the impactor M_i (coupled to the mass of the target, or proto-Uranus, M_t in order to keep the total mass constant), the angle at impact B, and the angular separation ϕ between the rotational axis of the proto-Uranus and the impactor's relative orbital axis. Additionally, some freedom was given to the speed of the impactor at the moment of contact v_c, but this was kept near to the mutual escape velocity of the system v_m,

$$v_m = \sqrt{\frac{2G(M_t + M_i)}{R_t + R_i}}, \tag{10}$$

where G is the gravitational constant, and R_t and R_i, and M_t and M_i are the radii and masses of the target (proto-Uranus) and impactor, respectively.

The lowest possible value of the impactor mass M_i that resulted in a sufficient axial tilt after a single impact event was desired; the lower the mass of the impactor, the more likely such an event is thought to be, given that smaller bodies are assumed to be more abundant in the early Solar System than those with significant mass. Additionally, the smaller the impactor mass, the less significant the

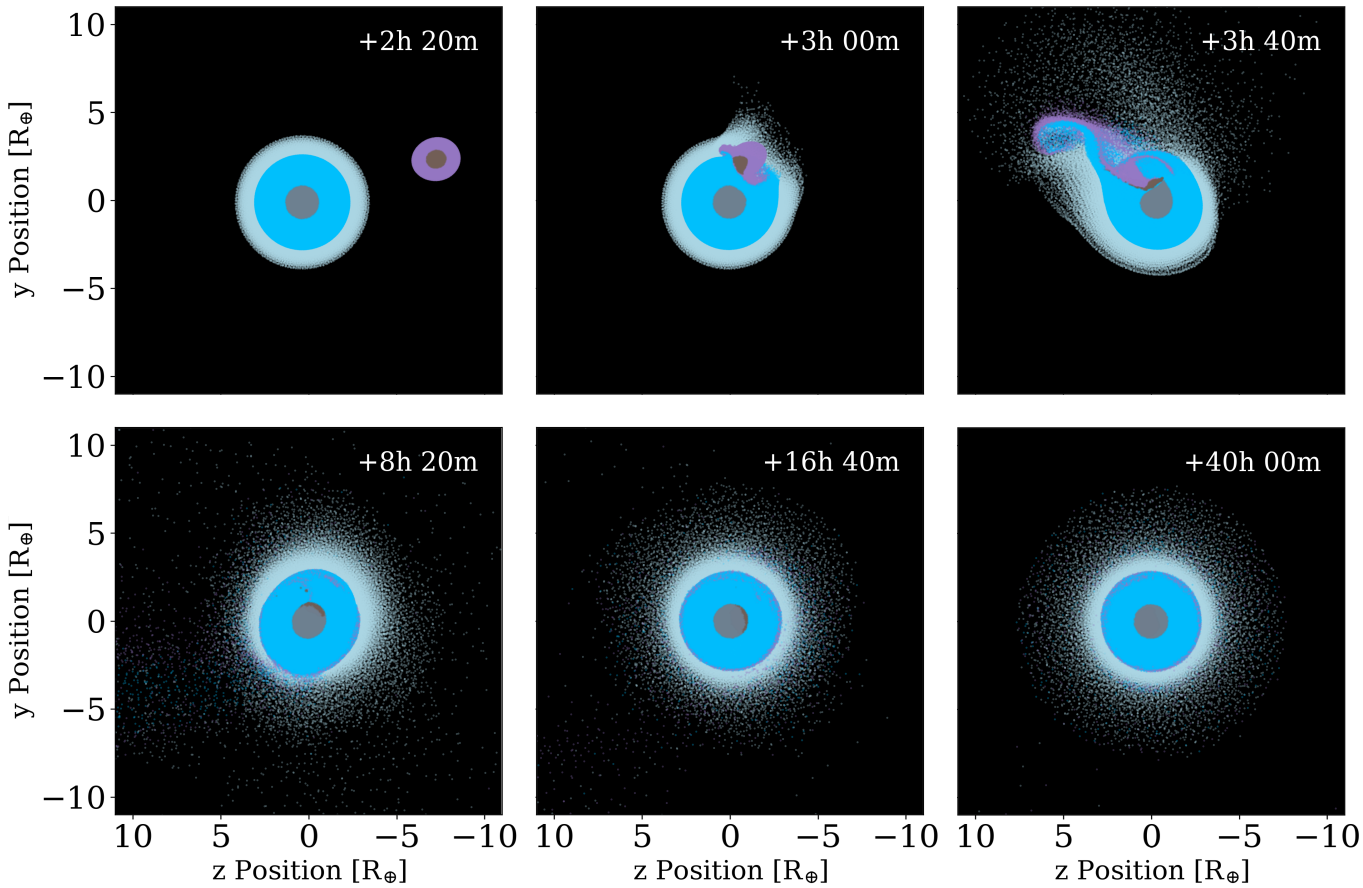

Figure 8. Cross-sectional snapshots of an impact from the 16.87-hour series with a 0.7 $M_\oplus$ impactor and an initial angular separation ϕ of 168°. The particles are coloured according to the standard colour scheme. An animation of this impact is available here.

material composition of the impactor; any error in judgement of its composition has as little bearing as possible on that of the post-impact Uranus since impactor material will comprise only a small fraction of the impact remnant.

3.1 Concurrent Series of Simulations

The rotation of each proto-Uranus was initially established with the hemispherical method until measurements with Equation 9 agreed with a rotation period of about 16.87 hours. This required giving each proto-Uranus at least two velocity kicks when requesting a period of about 15 hours. With the impactor mass varying between different simulations, the corresponding proto-Uranus that was generated for each new impactor was required to be spun up in this way. It was because of this repeated spin-up step that the rigid-body-like method was implemented; eliminating the need to wait (at least twice) for the hemispherical method to finish settling into steady-state rotation each time a new impactor mass was investigated. The new method set the proto-Uranus spinning with more or less exactly the period that was requested. However, spinning up the proto-Uranus in this way to an *expected* period of 16.87 hours yielded a measurement with Equation 9 not of 16.87 hours but somewhere closer to 25.31 hours. In order to *measure* a period similar to 16.87 hours, a requested period of 11.25 hours was needed. By qualitative inspection of the motion of a handful of particles within the proto-Uranus, the true period of rotation in this case was closer to 11.25 hours; the requested value. The requested value was therefore taken to be the more accurate metric of rotation.

In light of this disparity, simulations investigating the post-impact axial tilt continued with two concurrent series of simulations; one with pre-impact rotation periods which were *measured* to be 16.87 hours (but were actually spinning with a period of 11.25 hours), and the other with an *actual* rotation period of 16.87 hours (but were measured to be spinning with a period of roughly 25 hours). In the impact simulations carried out within each series, the 'free' parameters were varied as if the pre-impact rotation was not an issue. The two series qualitatively correspond to different assumed initial states of the same proto-Uranus and are kept distinct in the results presented here. The tabulated results from the two series are provided in Appendix B. The implications these differences have in regard to contextualising these simulations to the actual history of Uranus is left to the discussion in Section 4.3.

In each series, the same impactor masses were considered, ranging from 0.5 to 1.75 $M_\oplus$. The 11.25-hour series considered two additional impactors with masses of 0.1 and 2 $M_\oplus$. The 0.1 $M_\oplus$ impactor was quickly deemed insufficient to produce any meaningful tilt and was not therefore transferred into the 16.87-hour series when the split was made; a choice substantiated by the low axial tilts produced by the 0.5 $M_\oplus$ impactor in the 16.87-hour series.

Snapshots of an impact from the 16.87-hour series with a 0.7 $M_\oplus$ impactor and an initial angular separation ϕ of 168° are presented in Figures 8 and 12.

3.2 Impact Angle

The angle B between the impactor's relative position vector and the horizontal axis, at the moment of contact, is directly related to how much angular momentum is imparted onto the protoplanet. In a head-on collision, the impact angle is 0° and there is no orbital angular momentum of the impactor relative to the proto-Uranus, and therefore the protoplanet's rotational axis cannot be drastically redirected by the impact. With a perfectly grazing impact, at an impact angle of 90°, the impactor has the highest relative orbital angular momentum a collision could have, but very little angular momentum is transferred to the proto-Uranus since the bodies only touch tangentially. The amount of angular momentum that is delivered by the impactor will rise and fall for impact angles ranging from 0 to 90°. The value of B at which the most angular momentum is delivered to the protoplanet is therefore the most efficient impact angle for a given impactor mass. The minimum required impactor mass that sufficiently tilts Uranus is lowered by considering impacts at or near this most efficient impact angle; e.g. at low impact angles, just shy of head-on collisions, the impactor's mass would need to be enormous (or have a significant impact velocity, if it were not mostly fixed) in order to deliver enough angular momentum to overwrite the protoplanet's original rotation.

For some values of B, and in fact all values beyond a minimum, the trajectory of the impactor into the protoplanet is such that the impactor only substantially collides with the atmosphere before exiting the other side, in what is known as a 'hit-and-run' style impact. The partially stripped impactor may then re-collide some time later, albeit with less kinetic energy and mass. It was found that these types of impacts occurred above an impact angle of approximately 35°, below which the impactor is able to collide sufficiently with the icy layer such that it is almost entirely absorbed into Uranus, delivering a substantial amount of its angular momentum. Therefore, in most of the simulations carried out, the impact angle was set to around 30° to ensure maximal angular momentum transfer thus allowing for a minimum constraint on the impactor mass to be found.

3.3 Density and Temperature Profiles of the Impact Remnant

The thermal expansion of the protoplanet's atmosphere, as well as any vaporised material from the impactor or the rest of the protoplanet itself, means the size of the protoplanet changes considerably as a result of a giant impact. The dynamics of the impact remnant's rotation can only be defined once the remnant itself is well-defined. By generating density and temperature profiles from determining the radial separation of particles from the centre of mass of the system, the radial extent of the remnant could be found. In Figure 9, the density profile of the remnant depicted in the last frame of Figure 8 is presented. Unlike the pre-impact density profile, which is denoted with a black line in the figure, the remnant's profile is well-defined out to approximately 8 $R_\oplus$; a factor of 2 larger than the protoplanet prior to impact. The point at which a given remnant's density profile truncates was taken to be its radius. This point typically coincided with the particle density dropping below a value of around 2 kg m^{-3}. The qualitative assessment of size deduced from cross sections like those depicted in Figure 8 also agreed with this analysis. It should be noted that the particles' maximum smoothing length h_{max} might bias the fluid simulation towards more globular behaviours the higher h is permitted to be; h_{max} was set to 0.4 $R_\oplus$ in the simulations, but tuning this may result in slightly different calculations of the remnants' radii.

The differentiation of material layers in the remnant can be seen in Figure 9 as the stepping of the density profile. The positions of the steps suggest core-mantle and mantle-atmosphere boundary radii, for this impact, of about 1 and 2.5 $R_\oplus$, respectively. In all of the hit-and-merge impacts simulated, i.e. those with impact angles below 35°, the radial profiles looked similar.

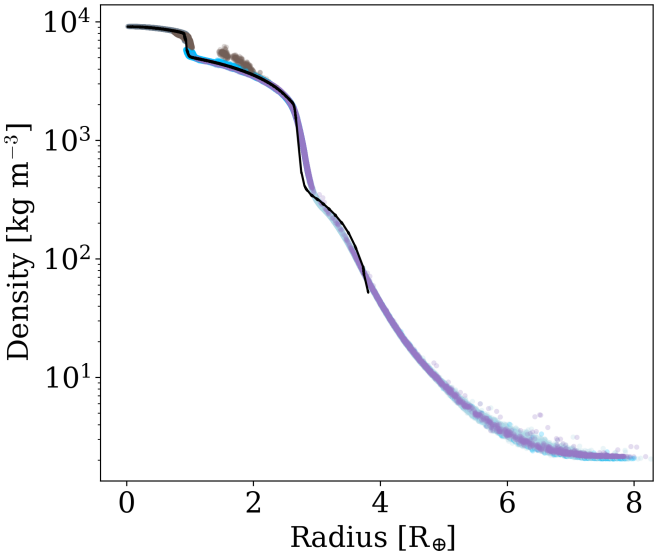

Figure 9. The density profile of the impact remnant from the simulation depicted in Figure 8. Each particle's density is plotted with a colour according to the standard colour scheme. The black line represents the protoplanet's pre-impact density profile.

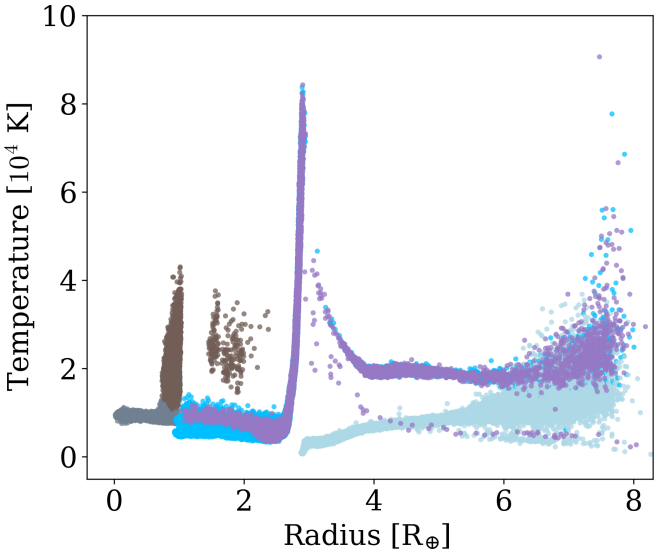

Figure 10. The temperature profile of the impact remnant from the simulation depicted in Figure 8. Each particle's temperature is plotted with a colour according to the standard colour scheme.

In temperature profiles of the impact remnants, such as Figure 10, the ice material from both the impactor and proto-Uranus can be seen to be reasonably well mixed beyond 2 $R_\oplus$; within this radius, the impactor ice is dwarfed in abundance by ice from the protoplanet. Cross sections of the remnant show an apparent shell of ice originating from the impactor sitting at the top of the ice layer, possibly representing the shell of material that is hypothesised to be causing the lack of observed heat flow from the core of Uranus today. The band of particles stretching up to 8×10^4 K in Figure 10 is this shell

of material, located at about $3\,R_\oplus$ from the centre and thus well within the current radius of Uranus ($3.98\,R_\oplus$). The impactor's rock is almost entirely delivered to the edge of the core, and cross sections show that it is not isotropic; it is concentrated on the side of the core that was closest to the impact site and subsequently rotates with the core. If the impactor's core has magnetic properties, this could explain the apparent observed offset of Uranus' magnetic dipole from the rotation axis (Warwick et al. 1986). The rocky material from the protoplanet that is in the centre of the remnant is of a similar temperature to its pre-impact state, with rock temperatures only increasing near the delivered impactor rock, which is significantly hotter than the ice material near the core-mantle boundary. A small amount of impactor rock is mixed into the mantle of the remnant, and does not find its way to the bulk of the rocky material in the core. Beyond the hot shell of ices lies the diffuse material; predominantly composed of the atmospheric material from the protoplanet, but with a mixture of ices originating from both pre-impact bodies.

The large temperatures and diffuse material beyond Uranus' current radius suggest that cooling and contraction could play significant roles in the dynamics of Uranus' rotation as it evolved from the post-impact state to the current day. This helped inform the calculations and results of the remnant's period of rotation (see Section 3.5).

3.4 Axial Tilt

With the impact remnant defined, the rotational dynamics of the body could then be analysed. Only particles located within the defined radius of the remnant were considered in calculations of its axial tilt and period of rotation. The angle θ between the pre-impact protoplanet's rotational axis and the post-impact remnant's rotational axis was defined as the axial tilt arising from a given simulation. This was calculated from the definition of the vector dot product,

$$\vec{L}_i \cdot \vec{L}_f = |\vec{L}_i|\,|\vec{L}_f| \cos\theta, \tag{11}$$

$$\cos\theta = \frac{\vec{L}_i \cdot \vec{L}_f}{|\vec{L}_i|\,|\vec{L}_f|}, \tag{12}$$

where $\vec{L}_i$ and $\vec{L}_f$ are the initial and final angular momentum vectors of the protoplanet and remnant, respectively.

Additionally, the axial tilt of each material component was found by only considering a subset of the remnant's particles in the calculation of $\vec{L}_f$ with Equation 6; material-specific axial tilt is thought to be a better indicator of the remnant's rotation. The atmosphere and mantle are most significantly disrupted by the impact and, as such, are imparted with most of the impactor's angular momentum. Since the mass of the atmosphere is comparable to the mass of the impactor, the atmosphere responds the most 'efficiently' to the impact and can end up with an axial tilt much closer to the initial angular momentum separation ϕ than the deeper layers can. With the mantle often being at least 10 times the mass of the impactor, it is generally less responsive to the delivered angular momentum than the atmosphere is. The rocky core is the most protected layer from the impact, and the dragging of the core by ices at the core-mantle boundary is the dominant mechanism which tilts its rotation, but some angular momentum is also transferred from the impactor's rock which finds itself on the side of the core after sinking through the ice layer. Since the mantle is the most massive component of the remnant and carries the bulk of the planet's angular momentum, the transfer of angular momentum between the layers as the planet equilibrates towards a rotational steady state is thought to cause the rotation of the atmosphere and rocky core to tend towards towards the rotation axis of the ice mantle. Therefore, the axial tilt of the mantle layer is expected to be a better indicator of the steady state axial tilt when compared to the tilt of the entire particle subsystem, and this value is used as the key indicator of each simulation.

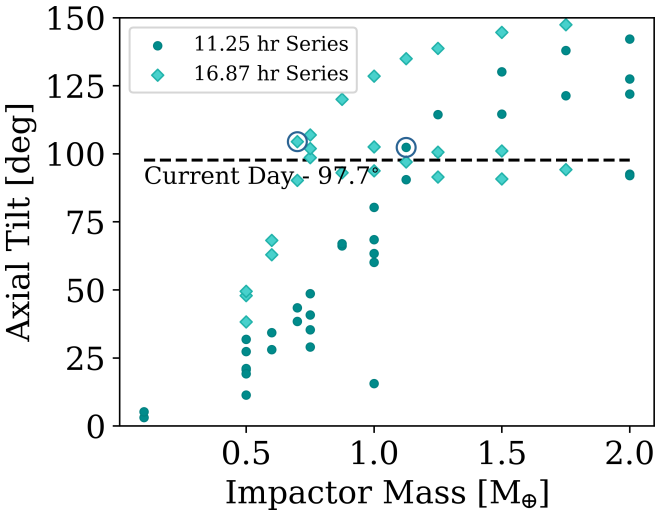

Figure 11. The axial tilts of the ice mantle layer in each of the post-impact remnants against the mass of the impactor. The two series of simulations are differentiated by colour and marker shape. The dashed line is the current value of Uranus' axial tilt. The circled data points refer to the lowest impactor masses in each series to surpass the axial tilt threshold, and correspond to masses of $0.7\,M_\oplus$ and $1.125 M_\oplus$.

The axial tilts of the ice mantle layer versus the mass of the impactor are depicted in Figure 11. Data points that sit near or above the dashed line, which corresponds to the observational value of Uranus' 97.77° axial tilt, are simulations that achieved the required tilt. The different tilts acquired by each different impactor mass are a result of different initial angular separation values ϕ of the angular momentum axes. Initial simulations for a given impactor mass were conducted with a baseline ϕ value of around 158°. For simulations that were followed up with subsequent tweaks, like most of those from the 16.87-hour series, the ϕ value was adjusted to minimise the difference between the simulated and required axial tilt of Uranus. Impactor masses that require ϕ values above 180° to obtain a 97.77° axial tilt are deemed insufficient, since ϕ is symmetric around 180°.

For the 16.87-hour series, the minimum impactor mass that satisfied this axial tilt was found to be $0.7\,M_\oplus$, which had a ϕ value between 158 and 168°. For the 11.25-hour series, the minimum impactor mass was found to be $1.125\,M_\oplus$, with a ϕ value between 148 and 158°. The axial tilt of the rocky core of the planet was found to closely match that of the mantle, and the lower bounds on the impactor mass are unchanged when considering either component. As expected, the atmospheric component is more responsive to the impact and can reach axial tilts of 97.77° with slightly lower impactor masses; requiring masses above 0.5 and $1\,M_\oplus$ for the 16.87 and 11.25-hour series, respectively.

The simulations that exceeded the required axial tilt but were not followed up with simulations with a more accurate ϕ value are assumed to represent configurations where a suitable ϕ value exists, namely the heaviest impactors in the 11.25-hour series. This is evidenced by impacts from the 16.87-hour series with impactor masses above $0.75\,M_\oplus$ which were followed up and shown to produce the necessary axial tilt.

Figure 12 shows the changing rotation axis of the protoplanet

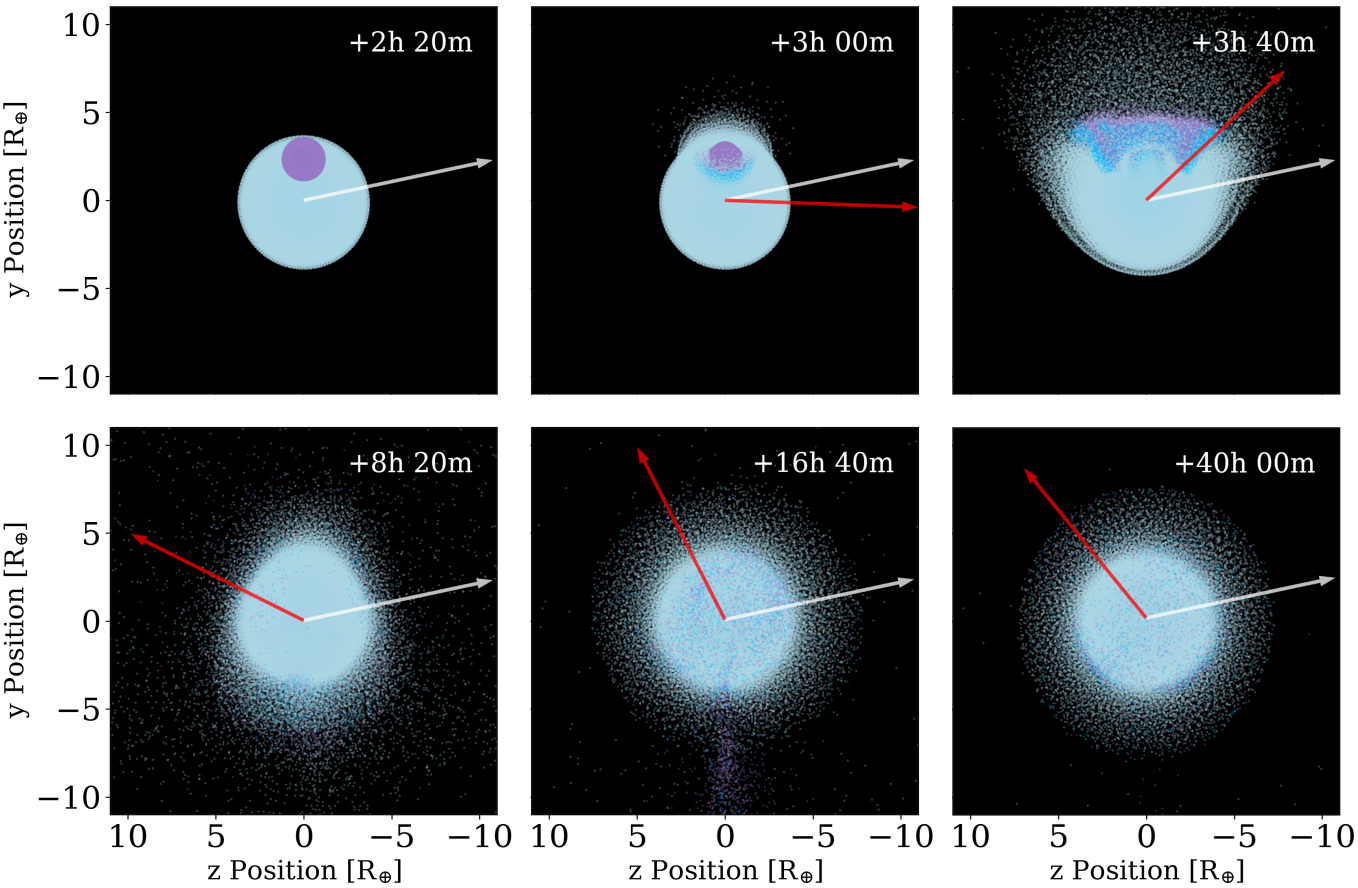

Figure 12. Snapshots of an impact from the 16.87-hour series with a 0.7 $M_\oplus$ impactor and an initial angular separation ϕ of 168°. This is a side view of the same snapshots as in Figure 8. The white arrow indicates the rotational axis (parallel to the orbital axis) of the protoplanet before impact, and the red arrow indicates the changing rotation axis of the ice materials during the impact event. Note how the two arrows are eventually separated by approximately 98°, as required. The particles are coloured according to the standard colour scheme. An animation of this impact is available here.

during a giant impact with a 0.7 $M_\oplus$ impactor, as indicated by the coloured arrows. The white arrow corresponds to the pre-impact rotation axis of the protoplanet, which is also parallel to the protoplanet's orbital axis. The remnant is seen to exhibit a permanent change in the direction of this rotation axis that corresponds to an axial tilt of roughly 104°, which is in reasonable agreement with the required value. An animation of this impact is available from Appendix A.

3.5 Period of Rotation

The periods of rotation of each impact remnant are calculated with Equation 9 while considering all particles in the remnant. The calculation is sensitive to particles with larger angular momentum, i.e. those that are spinning reasonably fast and/or reasonably far away from the centre, and so the rotation periods can be skewed towards those of the diffuse atmosphere. Figure 13 shows the remnants' periods of rotation versus the impactor mass for both simulation series.

In the 11.25-hour series, the remnant period of rotation initially rises with impactor mass before reaching a turning point around 0.875 $M_\oplus$, after which higher impactor masses induce quicker rotation in the remnant. In order to tilt the rotational axis to an angle of 97.77° from the orbital axis, and in fact to any angle between 90 and 180°, an impactor must strike the target in the hemisphere that is rotating towards it; the rotation of the target must switch from prograde, i.e. rotation in the same sense as its orbit, to retrograde, i.e. rotation in the opposite sense to its orbit, when projected onto the orbital plane. As such, the average motion of all particles in the target must be redirected against their original direction. From Figure 13, it can be seen that when the impactor is of relatively low mass (0.1 $M_\oplus$), it struggles to deliver any meaningful amount of angular momentum to the target and thus barely affects the period of rotation of the impact remnant. With larger impactor masses (0.5 to 0.875 $M_\oplus$), the angular momentum that is delivered to the target can start to negate the pre-existing angular momentum thus reducing the speed of rotation and increasing its period. With further increasing impactor mass (0.875 to 2 $M_\oplus$), the angular momentum delivered by the impact can start to spin the target in the opposite direction with increasing speed, or decreasing period, which explains the downward trend seen at these impactor masses.

As mentioned in the analysis of the remnants' temperature profiles, the rotation of the impact remnant is expected to change over time as it settles into a steady state. It is expected that as the remnant cools and the atmosphere contracts, the radial extent of the remnant will decrease. By conservation of angular momentum, this would imply the speed of rotation should increase, thus decreasing its period. The exact processes by which the planet would conserve angular momentum and subsequently spin up are beyond the scope of this study, but in an attempt to estimate their effects, crude models of contraction were implemented.

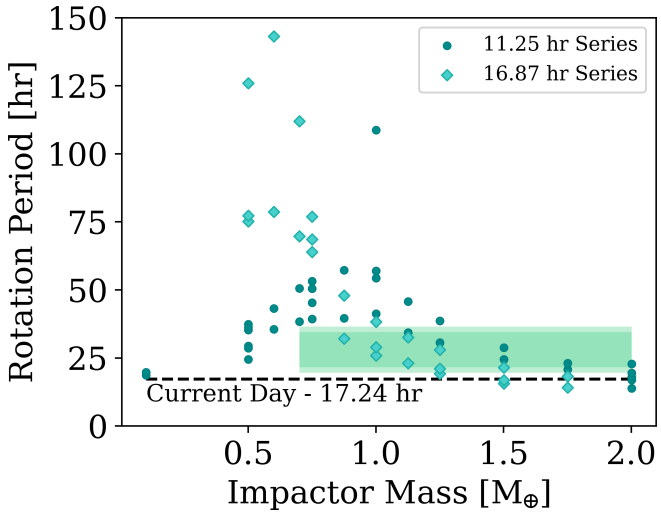

Figure 13. The periods of rotation of each impact remnant against the mass of the impactor. The two series of simulations are differentiated by colour and marker shape, according to the legend. The dashed line is the current value of Uranus' rotation period. The highlighted region is an estimate of the range of period values that would be expected to evolve near to the dashed line as the remnant cools over time.

Since the current radius of Uranus is 3.98 $R_\oplus$, a first approximation to contraction was to map all the particles beyond 3.98 $R_\oplus$ from the remnant's centre into a 1 $R_\oplus$ thick shell, encasing the rock and ice layers and ending at Uranus' current radius. The thickness of this shell was determined by the depth of the atmosphere found in the model of current-day Uranus, as described in Section 2.3. With the altered system of particles, the periods of rotation were re-calculated and found to drop by about 10 to 20% of their original value. This means that the post-impact period can be approximately 10 to 25% larger than present and be expected to spin up near to the current period of Uranus after contraction.

In a second approximation to contraction, the ice and rock layers were compressed by approximately 25% in addition to the previous atmospheric contraction. The contraction amount was derived from the fact that the mantle should end where the newly compressed atmosphere begins (2.98 $R_\oplus$), which is approximately 75% of the way to Uranus' current radius. With this method, the periods of rotation dropped by approximately 50%, meaning the post-impact periods can be approximately double the current period of Uranus and still be expected to spin up to the observed rate of rotation.

These two contraction models inform the vertical bounds of the highlighted region in Figure 13, which denotes a range of acceptable remnant periods that might spin up to Uranus' current period for impactor masses which are sufficient to also tilt Uranus by at least the necessary amount. The minimum impactor masses that satisfy the axial tilt requirement of the remnant, 0.7 and 1.125 $M_\oplus$ for the 16.87- and 11.25-hour series respectively, do not fall with confidence into this region. The 16.87-hour series simulations of a 0.7 $M_\oplus$ impactor end, at best, with twice the maximum permitted period.

The highlighted region can be used to estimate a maximum impactor mass; if the remnant is tilted correctly, but spinning with a period below the highlighted region, it would be expected to increase the speed of its rotation beyond the value observed today, and potentially rule itself out as a possibility.

The impactor mass is not subject to equal constraints on its minimum and maximum value. The minimum value is assumed to be a hard limit that any impact must adhere to since these simulations are carried out with the most efficient angle at which to deliver angular momentum. A similar hard limit does not exist for the maximum impactor mass since by lowering the impact angle, an impactor with a larger mass may still be able to deliver the required angular momentum and tilt Uranus appropriately. Additionally, if the relative speed of the impactor is significantly less than the mutual escape velocity considered here, then more massive impactors are permissible. Therefore, any upper limits on impactor mass are relevant only to the specific impact angle and contact velocity studied, and higher masses are permitted as both the impact angle and/or approach velocity decrease.

Within the constraints of this study, impactor masses of approximately 1.75 $M_\oplus$ or higher are thought to be too massive to yield the current behaviour of Uranus.

4 DISCUSSION

4.1 Orbital Considerations of the Impactor

The simulations presented in this study neglect any context from the wider Solar System; the initial angular separation ϕ determines the approach of the impactor relative to the proto-Uranus, which has implications for the impactor's orbit or trajectory through the Solar System. It is reasonable to assume that the impactor originated from within the Solar System and is bound within its gravitational well; an extra-solar body would also make both the impact significantly less likely and the impactor's composition significantly less constrained. An example of how an impactor may be in orbit around the Sun such that it impacts the proto-Uranus with an impact angle B and angular separation ϕ is given in Figure 14b. For this example, the inclination α of the impactor's orbit relative to Uranus' orbital plane can be derived with the following equations,

$$\epsilon = (R_t + R_i)\sin(B), \tag{13}$$

$$\beta = \cos(\phi - 90^\circ)\epsilon = \sin(\phi)\epsilon, \tag{14}$$

$$\tan(\alpha) \sim \frac{\beta}{r_t}, \tag{15}$$

where β, ϵ, and r_t describe distances as shown in Figure 14. These equations show that there are some constraints placed, in certain scenarios, on the impactor's orbit given a combination of ϕ and B. It should, however, be noted that there is a high degree of rotational symmetry in the impact scenario, as there are equivalent impacts if the impactor is rotated around either the pre-impact rotational axis of the protoplanet $\vec{J}_t$, or the impactor's own relative angular momentum vector $\vec{L'}_i$. Figure 14b depicts only the very special case where the velocities of the two bodies are parallel at impact; in theory, the impactor could be travelling away from the Sun, or in the opposite sense to the protoplanet's orbit, or even down through Uranus' orbital plane and still yield the same, or similar, results.

In fact, the simple case that is depicted in Figure 14b can be deemed unlikely after analysis of the impactor's approach velocity. For an object to be bound in orbit around the Sun it should not exceed its escape velocity; which, at a distance of Uranus' mean orbital distance, is approximately 9.6 km s^{-1}. Given that Uranus' mean orbital speed is approximately 6.8 km s^{-1} (from NASA's Goddard Space Flight Center[3]), if the impactor were to be catching up to Uranus, i.e.

[3] http://nssdc.gsfc.nasa.gov/planetary/factsheet/

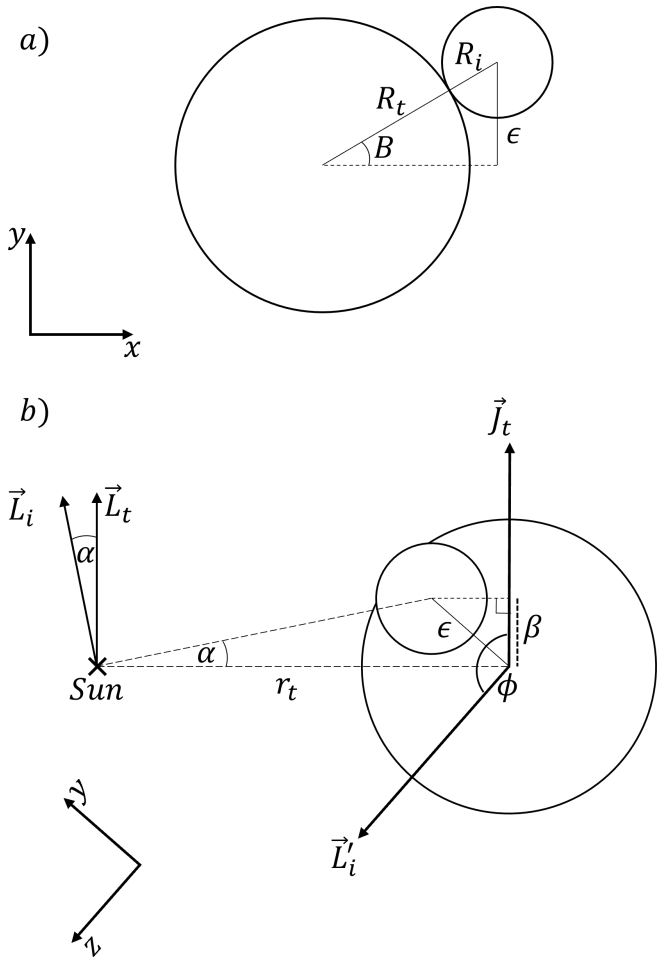

Figure 14. A schematic of the moment of impact contextualised to show one of many possible configurations of the impactor in its trajectory around the Sun. $\vec{L}_i$ and $\vec{L}_t$ are the orbital angular momentum vectors of the impactor and target relative to the Sun, and $\vec{L'}_i$ is the orbital angular momentum of the impactor relative to the target protoplanet. The magnitudes of these vectors are not to scale. Other quantities are as presented in previous figures, or calculated with Equations 13, 14, and 15.

orbiting in a similar sense to it like in Figure 14b, it could not exceed a relative approach velocity of about 2.8 km s^{-1} (= 9.6 - 6.8 km s^{-1}). Once the impactor is sufficiently close to the protoplanet its relative velocity is permitted to speed up as gravitational attraction accelerates the bodies towards each other, but far from Uranus' influence they would require relatively similar orbital velocities. The small speed of approach makes it difficult for the impactor to be sufficiently accelerated up to the mutual escape velocity, as required in the simulations carried out here. Additionally, two bodies of appreciable size and mass are unlikely to have been able to form on exceedingly similar orbits; the bodies would have almost certainly interacted, disrupting their formation, long before the impact could occur.

This seems to suggest that the impactor would have to take an unusual path through the Solar System in order to approach the protoplanet with the required separation of their angular momentum axes, as well as with an approach velocity that keeps the impactor bound to the Sun. An impactor that orbits the Sun in the opposite sense to Uranus would be allowed to have a maximum approach velocity of 16.4 km s^{-1} (= 6.8 + 9.6 km s^{-1}), which is more than double what is necessary to achieve the impact speeds that were simulated; it is however, highly unusual for planetesimal objects to be orbiting 'the wrong way' around the Sun since residual angular momentum from the protoplanetary disk would tend to generate similarly orbiting bodies. Fortunately, there is a potential mechanism which could be used to justify such an impactor taking peculiar orbits and potentially colliding with Uranus; the Jumping Jupiter scenario (Brasser et al. 2009; Nesvorný 2011). In this model of the early Solar System, a fifth ice giant is predicted to have been ejected from the system from a close encounter with the gas giants. While the mass of the hypothesised planet is predicted to be larger than Uranus' mass, and therefore much larger than the minimum impactor mass required from the simulations conducted in this study, the possibility of Jupiter playing a role in disturbing the trajectories of massive objects is promising for the impact hypothesis. The findings of Safronov (1972) also hint that a similar interaction between Jupiter and a slightly smaller body could, in theory, eject the latter onto a number of highly elliptical orbits which cross Uranus' path and become the impactor required to tilt Uranus on its side.

In any case, the impactor appears to require a reasonably elliptical orbit to feasibly deliver the angular momentum needed from an impact, which may harm the chances of such an impact occurring if any future understanding of bodies in the early Solar System acts to make this scenario less likely.

4.2 Rotational Period Interpretation

With these simulations, aside from the consideration of pre-impact rotation, the key difference from previous numerical studies on giant impacts with Uranus is the motivation for acceptable post-impact rotation periods. In most previous studies on the subject, the remnant's period of rotation was sought to be, at most, Uranus' current period, 17.24 hours; considering impacts that leave the remnant spinning as fast or faster than it is seen today. This was motivated by considerations of magnetic interactions between the remnant's core and orbiting or unbound material; angular momentum may be transferred away from the remnant and thus its rotation would be slowed and its period increased. Since the observational value of Uranus' period of rotation comes from measurements of the rotation of its magnetic field, the assumption that magnetic influences would act to change this value is reasonable. However, this also assumes a reasonably significant transfer of angular momentum. The ratio of post-impact to present-day rotation periods can be shown to be the same as the ratio of the corresponding angular momenta. Since most of the impacts considered in the previous literature leave the remnant spinning with periods of almost half the present value (Kegerreis et al. 2018), this implies the planet needs to lose nearly half of its angular momentum to magnetic interactions with nearby material. The remnants carry angular momentum on the order of 10^{36} kg m^2 s^{-1} and, assuming that the angular momentum is not transferred to a planet-sized mass of magnetic material and the fact that very little core material is ejected into orbit around the remnant, it is hard to imagine where the abundance of required magnetic material could originate from that could remove this angular momentum from Uranus.

The magnetic interactions in these previous works are also operating without the assumption that Uranus experiences an increase in angular velocity as it cools and contracts. In these studies, material beyond approximately 6 $R_\oplus$ is deemed to only be available for the formation of its satellite system, and so there is much less scope to consider the contractive effects on the remnant's rotation.

In the work presented here, and motivated by a similar discussion from Rufu & Canup (2022), the contraction of the remnant was deemed to be an important mechanism in the remnant's evolution

towards Uranus' current state. The decision to permit remnants that spin slower than the planet today is a significant deviation from some of these previous studies. The advantages of this consideration allow for the minimum impactor mass to be lowered which, in turn, increases the likelihood of such an impact occurring, and makes the impact hypothesis increasingly appealing.

However, the implications of a giant impact on Uranus' satellite system are important. They were neglected in this work to focus on constraining the effects of a giant impact on the planet itself, but it has been suggested by Rufu & Canup (2022) that some of the impacts presented in previous literature are insufficient to yield the expected behaviour of the combined system of Uranus and its moons. Considering the fact that impacts presented in past studies showcase impactors with much larger masses than $0.7 M_{\oplus}$, this may suggest that impacts of a young Uranus with a $0.7\ M_{\oplus}$ impactor are increasingly inconsistent with the observed system of Uranus' satellites. However, the way in which the disrupted bodies eventually evolve into the satellite system is still a topic of debate and, as detailed in Rufu & Canup (2022), it is left to future studies to constrain the necessary configuration of the Uranian system to agree with, or disprove, these impact results.

4.3 Rotational Approximations

The constraints on the minimum impactor mass are only sufficient to explain the axial tilt in Uranus and fail to also agree with rotational period calculations that would permit such an impact remnant to evolve into the current-day Uranus. Before the rotational period calculations are used to discredit these minimum mass observations, the validity of such calculations should be assessed.

When the calculated pre-impact rotation periods were found to be sufficiently different from their expected values, the interpretation of the calculated periods could be adjusted to acknowledge the disparity. The expected period agreed with the qualitative analysis of a handful of particles traced over a number of snapshots of the rotating protoplanet, and came out to be about 50% lower than the calculated value. The ratio between the expected and calculated rotational periods was consistent across several test spins and therefore the calculation was 'overruled' by the qualitatively derived value. Unfortunately, the same process could not be performed on the post-impact remnant since there was little coherence between each particle's period of rotation and, unlike the pre-impact protoplanet, the assumption that all the particles were co-rotating did not hold. The impact is expected to cause complex behaviours in the different layers of the remnant, and simply reducing the calculated period by the previously observed 50% would not be an appropriate assumption to make. By inspection of the remnants, even the particles within the diffuse atmosphere rotate at different speeds, and the remnants are therefore not rigid-body rotators.

If the remnants were given much longer to settle, the relative velocities of the particles might be brought into alignment and the calculated period of rotation may converge to a physically meaningful value. The viscous behaviours of each of the materials would need to be assessed in order to more accurately simulate the frictional transfer of angular momentum, as well as considering how the radiative cooling and contraction of the planet might play into its dynamics.

In the previous literature regarding simulations of impacts with Uranus, the method by which rotational periods from a collection of particles are calculated is not well documented, but some suggestion is made that the calculations are similar to those presented here (Equations 8 and 9). The same calculation method serves as a point of consistency between this and previous work, but the caveat that such calculations simplify the analysis should be emphasised. Additionally, the period of rotation quoted from observations of Uranus is derived from the rotation of Uranus' magnetic field (Warwick et al. 1986), which gives freedom to the mantle and atmospheric layers to have different rotation rates, or exhibit shear flow. Thus, a more accurate comparison between the impact remnant's rotation and Uranus' true rotation might be found by analysing the core rotation of the remnant. This is left as an area of further investigation alongside improved approximations of non-rigid body rotation.

5 CONCLUSIONS

SPH simulations were carried out to constrain the parameters defining a single giant impact that causes Uranus' axial tilt to reach its current value. In contrast to the previous literature on the problem, the implications of the planet's pre-impact spin were investigated. By considering impacts that most efficiently deliver angular momentum to the planet, the minimum impactor mass required to produce axial tilts as significant as that seen in Uranus today was found to be $0.7\ M_{\oplus}$. Under consideration of the long-term post-impact dynamics of the planet, namely the cooling and subsequent contraction of its vaporised and diffuse atmosphere, impactor masses above approximately $1.75\ M_{\oplus}$ may be too large to leave the planet rotating with its observed period of 17.24 hours. The motivations for acceptable post-impact periods differ from those in previous literature, and rotation periods of the impact remnant between approximately 21 and 35 hours are considered reasonable. The validity of the calculations used to determine the period of rotation of a non-rigid body was called into question and additional simulation series were carried out to observe if significantly deviated bounds on the impactor mass arose. In the new series with a more quickly rotating pre-impact planet, the minimum impactor mass rose to $1.125\ M_{\oplus}$.

Additionally, the geometry of the required collisions motivates the notion of the impactor's orbit through the Solar System being atypical of planet-sized bodies, but a gravitational interaction with one of the other giant planets in the Solar System could justify the unusual trajectory.

In agreement with the previous literature, the impacts establish a shell of impactor ice mixed into the top layer of Uranus' ice mantle component and may explain the thermal properties observed in the planet. If the impactor's core component exhibits magnetic properties, it is possible the observed offset of Uranus' magnetic axis from its rotational axis could be explained by the anisotropic deposition of impactor rock onto the protoplanet's core.

The implications of a giant impact on Uranus' satellite system are left to higher resolution studies that further investigate the impact hypothesis.

While not presented here, alongside this investigation into giant collisions inducing Uranus' tilt, there has been analysis of near-misses that deform Uranus tidally; with impactors that deliver angular momentum to the protoplanet via gravitational deformation (Verheul 2024). Reasonable axial tilts are obtainable with this mechanism, and it is possible that multiple near-misses or a combination of smaller collisions and near-misses could also explain Uranus' tilt. This avenue allows for the consideration of multiple impact events in Uranus' history, whether they are all collisional, all non-collisional, or a combination thereof, which broadens the scope of the research topic albeit with the decreasing probability associated with a chain of impact events occurring.

REFERENCES

Benz W., 1988, Comp. Phys. Comm., 48, 97
Boué G., Laskar J., 2010, ApJ, 712, L44
Brasser R., Morbidelli A., Gomes R., Tsiganis K., Levison H. F., 2009, A&A, 507, 1053
Gingold R. A., Monaghan J. J., 1977, MNRAS, 181, 375
Giuli R. T., 1968, Icarus, 8, 301
Guillot T., 2005, Ann. Rev. of Earth and Planet. Sci., 33, 493
Haldemann J., Alibert Y., Mordasini C., Benz W., 2020, A&A, 643, A105
Hamilton D. P., Ward W. R., 2004, AJ, 128, 2510
Harris A. W., 1977, Icarus, 31, 168
Harris A. W., Ward W. R., 1982, Ann. Rev. of Earth and Planet. Sci., 10, 61
Helled R., Anderson J. D., Podolak M., Schubert G., 2011, ApJ, 726, 15
Hubbard W. B., Macfarlane J. J., 1980, J. Geophys. Res., 85, 225
Hubbard W. B., Marley M. S., 1989, Icarus, 78, 102
Ida S., Ueta S., Sasaki T., Ishizawa Y., 2020, Nat. Astron., 4, 880
Kegerreis J. A., et al., 2018, ApJ, 861, 52
Kegerreis J. A., Eke V. R., Gonnet P., Korycansky D. G., Massey R. J., Schaller M., Teodoro L. F. A., 2019, MNRAS, 487, 5029
Korycansky D. G., Bodenheimer P., Pollack J. B., 1991, Icarus, 92, 234
Lubow S. H., Seibert M., Artymowicz P., 1999, ApJ, 526, 1001
Lucy L. B., 1977, AJ, 82, 1013
Monaghan J. J., Lattanzio J. C., 1985, A&A, 149, 135
Ness N. F., Acuna M. H., Behannon K. W., Burlaga L. F., Connerney J. E. P., Lepping R. P., Neubauer F. M., 1986, Science, 233, 85
Nesvorný D., 2011, ApJ, 742, L22
Nettelmann N., Wang K., Fortney J. J., Hamel S., Yellamilli S., Bethkenhagen M., Redmer R., 2016, Icarus, 275, 107
Podolak M., Cameron A. G. W., 1974, Icarus, 22, 123
Podolak M., Helled R., Schubert G., 2019, MNRAS, 487, 2653
Rogoszinski Z., Hamilton D. P., 2021, PSJ, 2, 78
Ross M., Graboske H. C., Nellis W. J., 1981, Phil. Trans. of the R. Soc. of Lond. Ser. A, 303, 303
Rufu R., Canup R. M., 2022, ApJ, 928, 123
Ruiz-Bonilla S., Eke V. R., Kegerreis J. A., Massey R. J., Teodoro L. F. A., 2021, MNRAS, 500, 2861
Safronov V. S., 1966, Soviet Ast., 9, 987
Safronov V. S., 1972, Israel Program for Scientific Translations,
Schaller M., et al., 2024, MNRAS,
Slattery W. L., Benz W., Cameron A. G. W., 1992, Icarus, 99, 167
Stewart S., et al., 2020, AIP Conf. Proc., 2272, 080003
Trac H., Pen U.-L., 2003, PASP, 115, 303
Verheul E., 2024, MSci Project Report
Warwick J. W., et al., 1986, Science, 233, 102

APPENDIX A: SIMULATION ANIMATIONS

An animation of the impact presented in Figures 8 and 12, as well as several other animations including different impactor masses and spin-up methods, can be found here, through the QR code below, or by request.

APPENDIX B: TABULATED SIMULATION DATA

Table A1. Tabulated data for the 11.25-hour series. The initial impact parameters are given in the first four columns, and the remnant properties are given in the last four columns; the period of rotation, and the axial tilts of the three material layers. The missing data for the last two 1 $M_\oplus$ simulations is a result of the high impact angle, and no impact remnant being properly defined before the end of the simulation.

M_i [$M_\oplus$]	B [°]	ϕ [°]	v_c [v_m]	P [hr]	θ_{rock} [°]	θ_{ice} [°]	θ_{atm} [°]
0.1	25	148	1	18.66	2.61	3.10	3.00
0.1	45	148	1.1	19.70	4.77	5.18	5.56
0.5	25	148	1	29.34	19.70	20.64	25.11
0.5	25	128	1.1	24.44	27.61	27.34	34.96
0.5	25	158	1.3	36.26	19.25	19.21	28.23
0.5	30	158	1.2	37.37	35.35	21.13	35.35
0.5	45	148	1	35.25	28.85	31.81	81.71
0.5	45	158	1.2	28.53	11.47	11.39	23.71
0.6	30	148	1	35.51	32.62	34.29	50.70
0.6	30	158	1	43.17	28.57	28.09	46.08
0.7	30	148	1	38.35	42.64	43.42	68.39
0.7	30	158	1	50.52	38.20	38.40	68.92
0.75	25	158	1.1	50.44	34.73	35.36	62.55
0.75	30	148	1	39.30	47.47	48.61	76.13
0.75	30	158	1.2	53.15	38.97	40.75	86.63
0.75	35	158	1.2	45.28	26.19	29.03	70.57
0.875	30	148	1	39.56	63.80	66.17	89.66
0.875	30	158	1	57.17	63.52	66.93	101.20
1	25	148	1	41.24	61.57	63.34	80.56
1	25	168	1.2	108.71	53.63	60.14	117.21
1	25	178	1	327.21	12.96	15.56	154.95
1	30	158	1.1	54.28	75.46	80.31	113.43
1	30	158	1.25	56.92	64.44	68.46	107.66
1	45	158	1.1	-	-	-	-
1	50	158	1	-	-	-	-
1.125	30	148	1	34.26	86.89	90.45	111.05
1.125	30	158	1	45.72	97.88	102.38	126.95
1.25	30	148	1	30.58	97.23	100.34	117.09
1.25	30	158	1	38.63	112.24	114.40	133.41
1.5	30	148	1	24.45	113.05	114.57	124.99
1.5	30	158	1	28.74	128.32	130.15	139.67
1.75	30	148	1	20.71	120.82	121.35	130.71
1.75	30	158	1	23.04	137.04	137.90	143.59
2	25	123	1	16.93	92.13	92.47	95.61
2	25	148	1	22.76	121.48	121.98	127.25
2	30	118	1	13.80	91.83	92.00	97.14
2	30	148	1	17.93	126.19	127.47	132.84
2	30	158	1	19.40	142.20	142.10	147.25

Table A2. Tabulated data for the 16.87-hour series. The initial impact parameters are given in the first four columns, and the remnant properties are given in the last four columns; the period of rotation, and the axial tilts of the three material layers. The simulation in bold denotes that which is depicted in Figures 8, 9, 10, and 12.

M_i [$M_\oplus$]	B [°]	ϕ [°]	v_c [v_m]	P [hr]	θ_{rock} [°]	θ_{ice} [°]	θ_{atm} [°]
0.5	30	158	1	75.12	46.78	47.90	70.79
0.5	30	158	1.1	77.27	46.16	49.51	88.96
0.5	30	168	1.1	125.87	34.60	38.20	102.46
0.6	30	158	1	78.61	65.33	68.20	100.01
0.6	30	168	1.1	143.10	56.75	62.91	130.47
0.7	30	158	1	69.72	88.19	90.20	119.08
0.7	**30**	**168**	**1**	**111.90**	**98.00**	**104.47**	**140.64**
0.75	30	158	1	63.84	95.81	98.59	124.72
0.75	30	160	1	68.56	98.51	101.94	128.07
0.75	30	163	1	76.92	103.98	106.92	134.3
0.875	30	138	1	32.10	91.72	93.04	103.19
0.875	30	158	1	47.88	117.88	120.02	132.35
1	30	132	1	25.82	91.87	93.71	103.80
1	30	140	1	28.92	100.87	102.49	113.84
1	30	158	1	38.22	126.64	128.55	139.76
1.125	30	130	1	23.05	95.75	97.00	104.30
1.125	30	158	1	32.53	133.93	134.97	142.06
1.25	30	121	1	19.14	89.9	91.47	98.18
1.25	30	130	1	21.01	100.02	100.57	108.67
1.25	30	158	1	27.97	137.41	138.71	145.21
1.5	30	114	1	15.55	89.06	90.73	95.29
1.5	30	124	1	16.76	101.28	101.04	106.03
1.5	30	158	1	21.48	145.17	144.56	148.63
1.75	30	114	1	14.06	94.44	94.16	98.41
1.75	30	158	1	18.25	146.03	147.39	150.38